

pubs.acs.org/JPCL Letter

Interference Effects in Micro-Raman Spectroscopy Enable Mapping of Chemical Gradients on an Elastomer Surface

Dhanusha T.N. Rathnayake, Nabeeha Malik, Sam Milone, Stephen A. Morin,* and Yinsheng Guo*



Cite This: J. Phys. Chem. Lett. 2024, 15, 8467-8476



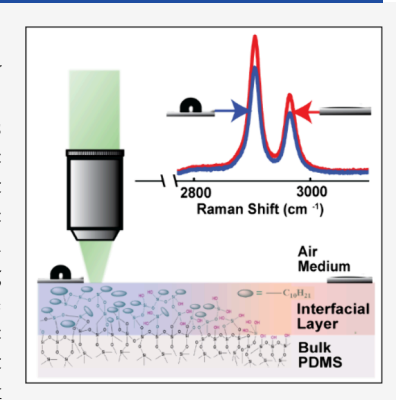
ACCESS I

III Metrics & More

Article Recommendations

SI Supporting Information

ABSTRACT: Chemically modified elastomer surfaces are important to many applications, including microfluidics and soft sensors. Sensitive characterization of the interfacial chemistry of soft materials has been a persistent challenge, given their structural and chemical complexity. This article reports a method to probe local chemical states of elastomer surfaces that leverages the interference effects observed in micro-Raman spectroscopy. Unexpectedly, systematic variations of Raman scattering intensity were observed across a chemical wettability gradient grafted to the surface of a poly(dimethylsiloxane) (PDMS) film. Specifically, hydrophobic surface regions with a high graft density of long-chain hydrocarbon molecules showed suppressed Raman intensity. An optical interference model that accounts for molecular filling and swelling of an interfacial glassy layer during chemical modifications of the PDMS surface quantitatively reproduces experimental observations. This work establishes the spectroscopic signatures of interfacial chemical modifications on elastomer surfaces and enables a noncontact optical probe of local chemical states at the micro- and nanoscale compatible with the complex interfaces of soft materials.



hemical functionalization of elastomer surfaces enables ✓ the rational control of properties (wettability, reactivity, adhesivity, etc.) that are essential to the performance of numerous soft, adaptive materials systems. 1-3 Examples of such designed properties and functions of soft material interfaces range from adsorption and adhesion, wetting, and molecular recognition, to biocompatibility and biomedical applications.4-6 While several strategies for the successful modification of elastomer surfaces have been reported, convenient analytical techniques that can provide localized physicochemical detail of these inherently heterogeneous systems have remained elusive, and the pace of discovery has been slowed. In this report, we work to address this longstanding constraint within the soft matter community by demonstrating a unique noninvasive, all-optical methodology that provides localized surface-chemical information. Specifically, we make use of interference effects from micro-Raman measurements together with a semiquantitative physical model to report the graft density of alkyl chains on modified PDMS.

Compared with prototypical systems in surface science, for example, the well-defined crystalline interfaces of inorganic materials or carefully prepared self-assembled monolayers, soft material interfaces are disordered and heterogeneous. It is this surface-chemical "complexity" that defines the *structure* and enables the unique *functions* of soft material systems. *Structurally*, surfaces of crystalline inorganic materials feature periodic atomic or molecular lattices with long-range interfacial order and a clear boundary between the bulk material and the surface adsorbed or bonded atomic and molecular species. On the contrary, interfaces of soft materials often feature labile

chemical bonding involving a wide variety of lightweight molecular components. The underlying soft materials are inherently disordered in their structural arrangement; no longrange order exists in a plane along their surface, and the boundary in the out-of-plane direction between the bulk and the chemically modified interface is often hard to delineate. *Functionally*, soft materials' interfaces are often designed with spatially heterogeneous patterns to enable desired functions. In many cases, these functions involve responses to external environmental factors and stimuli, enabled by temporally dynamic changes in the interfacial chemical states.^{7,8} The chemical composition and molecular architecture of these interfaces provide underpinnings for a wide variety of functional materials.^{9–11}

To enable our understanding of the structure and function of soft material interfaces, characterization approaches that are commensurate and compatible with their chemical complexity are indispensable. Desired measurement methods are expected to provide information on their chemical states, which are capable of resolving microscopic spatial variations, monitoring chemical changes over time, and remaining robust within complex chemical environments. These requirements render

Received: May 30, 2024 Revised: July 18, 2024 Accepted: August 6, 2024 Published: August 9, 2024





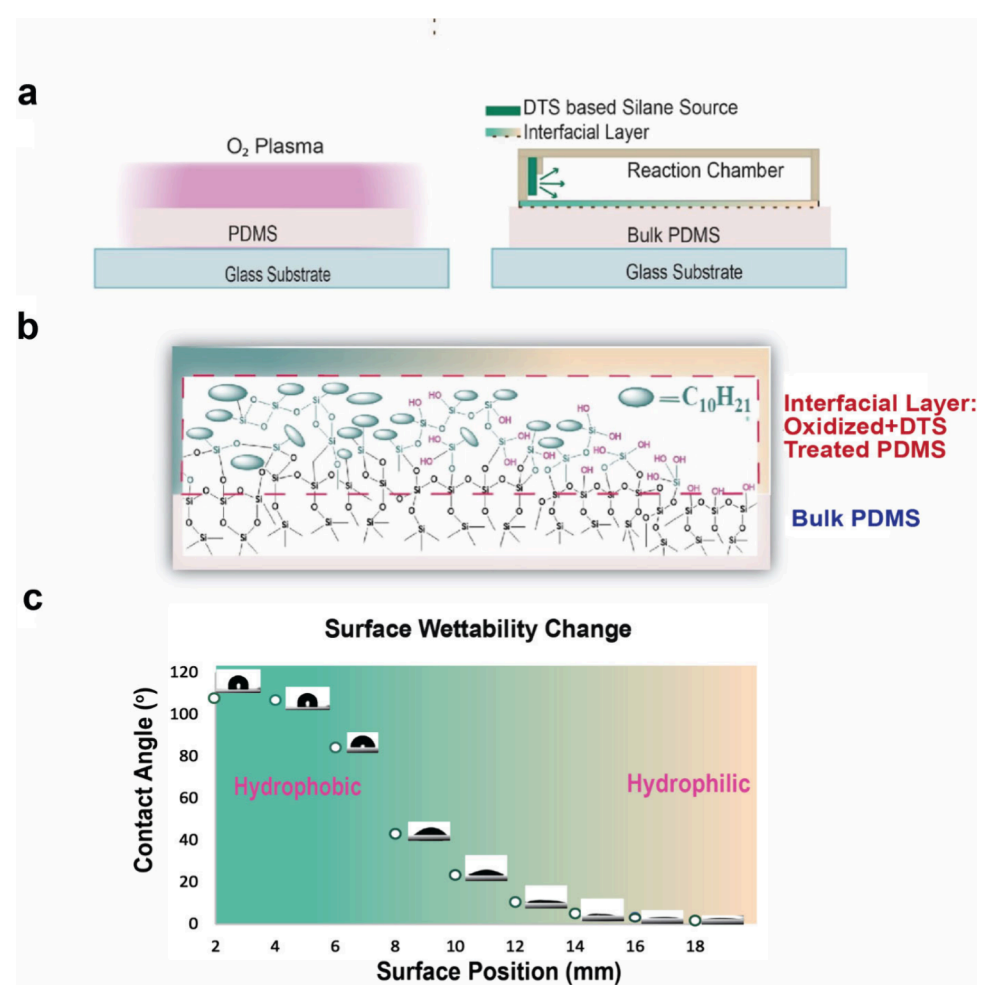


Figure 1. PDMS surface modification and contact angle measurements. (a) Formation of surface chemical gradient through chemical vapor deposition of silanes (DTS in mineral oil). (b) Cross section of molecular structures of the surface chemical gradient, controllably formed by DTS diffusion into the silica-like interfacial layer. (c) Contact angle variation along the chemical gradient of surface density of deposited silane. Optical images of contact angle measurements using water droplets are shown alongside the contact angle.

the characterizations of soft materials' interfacial chemical states challenging.

Standard surface characterization tools/methods such as energy dispersive X-ray spectroscopy (EDX) and X-ray photoelectron spectroscopy (XPS) contribute to our understanding of the elemental distribution on soft materials' surfaces, with a micrometer-to-submicrometer spatial resolution. However, as core-level spectroscopies, their sensitivity to detect and distinguish/differentiate molecular details from light elements is limited. The similarly natured organic substrate bulk and lack of a sharply defined boundary further add to their limitations in cleanly revealing interfacial chemical states. In addition, their vacuum operational environments preclude the possibility of in situ measurements. Sample loading in the vacuum chamber alone might perturb the sample chemical states. For instance, condensation of Si-Si and Si-O by eliminating water and/or mechanical strain has been reported to induce hydrophobic recovery of chemically modified elastomer surface, even before the start of the XPS analysis.¹² On the other hand, contact angle (CA) measurements reveal the surface chemical states from the perspective of the surface wettability profile. 13 Its recently developed variant, surface wettability visualization (SWAV), visualizes spatial variations of surface wettability using nebulized

microdroplets.¹⁴ However, these methods yield limited spatial resolution at the millimeter-to-submillimeter level, constrained by the minimum volume of droplets.

To bridge the gap in characterization approaches of soft material interfaces, we report here the optical signatures of chemically modified elastomer interface measured in Raman spectroscopy. Our measurement results enabled us to establish an analytical and numerical model of the optical properties of the chemically modified interfacial layer. The integrated measurement and modeling approach developed in this work opens a new perspective to address interfacial complexities in soft materials.

METHODS

Experimental Setup for Chemical Gradient Deposited on PDMS Surface. Chemical gradients on the surface of the gradient have been fabricated by the previously reported method. PDMS, which is widely used as an elastomer for its inertness and flexibility, was cured in the thin film form at a thickness of 500 μ m and oxidized to activate and create hydroxyl groups on the surface for further chemical modifications. Decyltrichlorosilane (DTS) was selected as the volatile molecule to stage the silane source for one-dimensional (1D) gradient deposition via the chemical vapor

deposition technique. Figure 1a demonstrates the experimental setup for this modification on a PDMS surface using a 3D printed chamber incorporating a silane source, which allowed the deposition with the flux of volatile molecules. Figure 1b illustrates the change in the density of deposited DTS. The surface was modified by DTS diffusing on a silica-like layer, forming an interfacial layer with varying thickness.

PDMS Fabrication. The ratio of 10:1 base to curing agent was mixed from a Sylgard 184 kit to formulate the PDMS at the required mechanical conditions. After that, the mixture was degassed under vacuum for approximately 20 min in order to remove any air bubbles. On a Silicon wafer, cleaned with Deionized (DI) water, Isopropanol, and Acetone, respectively, and dried with N_2 gas, the degassed mixture of PDMS was cast over by the universal applicator (Zethner) at the thickness of 500 μ m and was placed in the 60 °C oven for 2 h.

PDMS Oxidation. PDMS was cut into 1×1 in., and the side facing the silicon wafer was flipped up to expose it for oxidation. Precleaned glass slides were used as the substrates for the samples. The parameters selected on the O_2 plasma chamber (Plasma Etch Inc., Carson City, NV, model no. PD-25 Series) were 60% power and ~200 mTorr pressure for 60 s to oxidize the surface by creating silanol groups on the surface.

Chemical Vapor Deposition of DTS. For 1D Gradients Synthesis, a 3D printer chamber at the dimensions of $(40 \times 18 \times 10 \text{ mm})$ was used to stage a silane source for vapor deposition with a dimension room of $(30 \times 15 \times 8 \text{ mm})$ to hold enough air to derive the flux of volatile molecules along the length of the chamber.¹⁴

DTS (Gelest) is used as a volatile alkyl-based silane molecule diluted with Mineral oil in a 1:10 ratio. 15–20 μ L of the silane solution is used in order to fully wet the filter paper setting on the front end of the chamber to be used as a Silane source. After the filter paper was wetted with the silane solution, it was placed on the oxidized PDMS substrate in an inverted position for DTS deposition through the Chemical Vapor Deposition (CVD) technique for 1 min. After DTS deposition, samples were washed with warm (\sim 60 °C) water for 30 s and dried with N₂ gas.

Raman Spectroscopy. Raman spectroscopy measurements were conducted by using a custom-built confocal micro-Raman apparatus. A single-frequency continuous wave laser provides Raman excitation at 532.176 nm (Coherent Verdi V2). The excitation laser is coupled into a custom-built microscope using a band-pass filter of a volume holographic grating (VHG) filter set. A microscope objective is utilized to focus the excitation laser on the sample surface, and the backscattering geometry was used to collect the Raman signal using the same microscope objective. A Nikon 60X 0.70 NA (Numerical Aperture) microscope objective was used to acquire native PDMS and chemically modified PDMS Raman spectra. The acquired time was 60 s. The VHG band-pass filter also acts as a dichroic to keep the laser line out of the detection path. The laser line is further suppressed by more than 9 orders of magnitude with a spectral notch having a full width at half-maximum at around 7 cm⁻¹ above and below 0 cm⁻¹ using three-volume Bragg grating notch filters. The filtered signal is fed into an IsoPlane-320 spectrometer, dispersed by a grating with a specific grooves/mm value (1800 grooves/mm), and collected by a thermoelectrically cooled (liquid nitrogen-cooled) charge-coupled device (CCD) (PIXIS-BRX400). 15 The higher grating groove density spreads light over a larger region of the CCD, enhancing the spectral

resolution. Raman scattering with a Stoke's shift from 18 to 3200 cm⁻¹ was collected.

Water Contact Angle Measurements. The surface wettability of native PDMS, chemically modified PDMS (with DTS modification), and unmodified PDMS (without DTS modification) was evaluated by measuring the mean water droplet contact angle of the static drop dispersed on the substrate surface. For contact angle analysis, the sample was placed on the stage of attention of a Theta contact angle goniometer to analyze the change in contact angle along the gradient. The reference liquid used is the nano pure water droplets, and a droplet of 0.3–0.5 μ L volume (or ~0.4–0.5 mm radius) was used. For collecting contact angle values, the baseline was adjusted to automatic with 11 frames per measurement. The solid phase selection of PDMS and the light phase is assigned to be air, and the distance between two consecutive data points is ~2 mm.

Optical Modeling. We used the transfer matrix method for optical interference calculations. As a consistency check, we first reproduced the Raman enhancement of graphene on SiO₂/Si substrates due to optical interference (Supporting Information Figure S5). 16 For our elastomer surface calculations, the previously reported refractive indices of PDMS and silicon dioxide (SiO₂) were used. The refractive index of PDMS is around 1.4 (moving from wavelength from 532 to 700 nm, the refractive index will decrease from 1.44 to 1.42). 17-20 Plasma-oxidation of PDMS results in a thin silicalike skin layer,²¹ and the refractive index of SiO₂ was decreased from 1.46 to 1.45. 20-22 The refractive index of DTS is around 1.45 (Thermo Fisher Scientific, Gelest). The surface was modified by DTS diffusing on a silica-like layer, forming an interfacial layer with varying thickness and refractive index. The refractive index of SiO₂ was used as the refractive index of the interfacial layer. The Silica-like layer is denser than PDMS, and normal silica glass is denser than the silica-like layer.²³ Therefore, we considered the air and interfacial layer interface refractive indices to be between air $(n_{air} = 1)$ and glass $(n_{glass} = 1)$ 1.5). The interfacial layer refractive index can vary between the refractive index of PDMS and the Silica-like layer. Calculations were done using the Python "tmm" package (Supporting Information section 4).

In this work, Sylgard 184, a widely used silicone-based elastomeric polymer composite material, is selected as the model system for the characterization of local interfacial chemical states. Commercialized under the name Sylgard 184, this model system is a composite of polydimethylsiloxane (PDMS) and 30–60 wt % fumed silica. This composite elastomer is also broadly referred to under the name of its polymer base as PDMS; we adopt this denotation hereafter.

PDMS is extensively explored due to its remarkable properties including physiological indifference, biocompatibility, chemical stability, mechanical properties, gas permeability, excellent optical transparency, and adaptability. PDMS is hydrophobic in nature. When it is oxidized by oxygen plasma, a silica-like layer is created on the exposed surface, the thickness of which increases with plasma power and treatment time. Perminal hydroxyl groups are also expected to be generated on the surface while oxidation activates the surface for further chemical modification. This modification imparts new properties, such as increased hydrophilicity, improved adhesion, and altered mechanical behavior. Spatiotemporal control of surface chemical modifications enable the formation

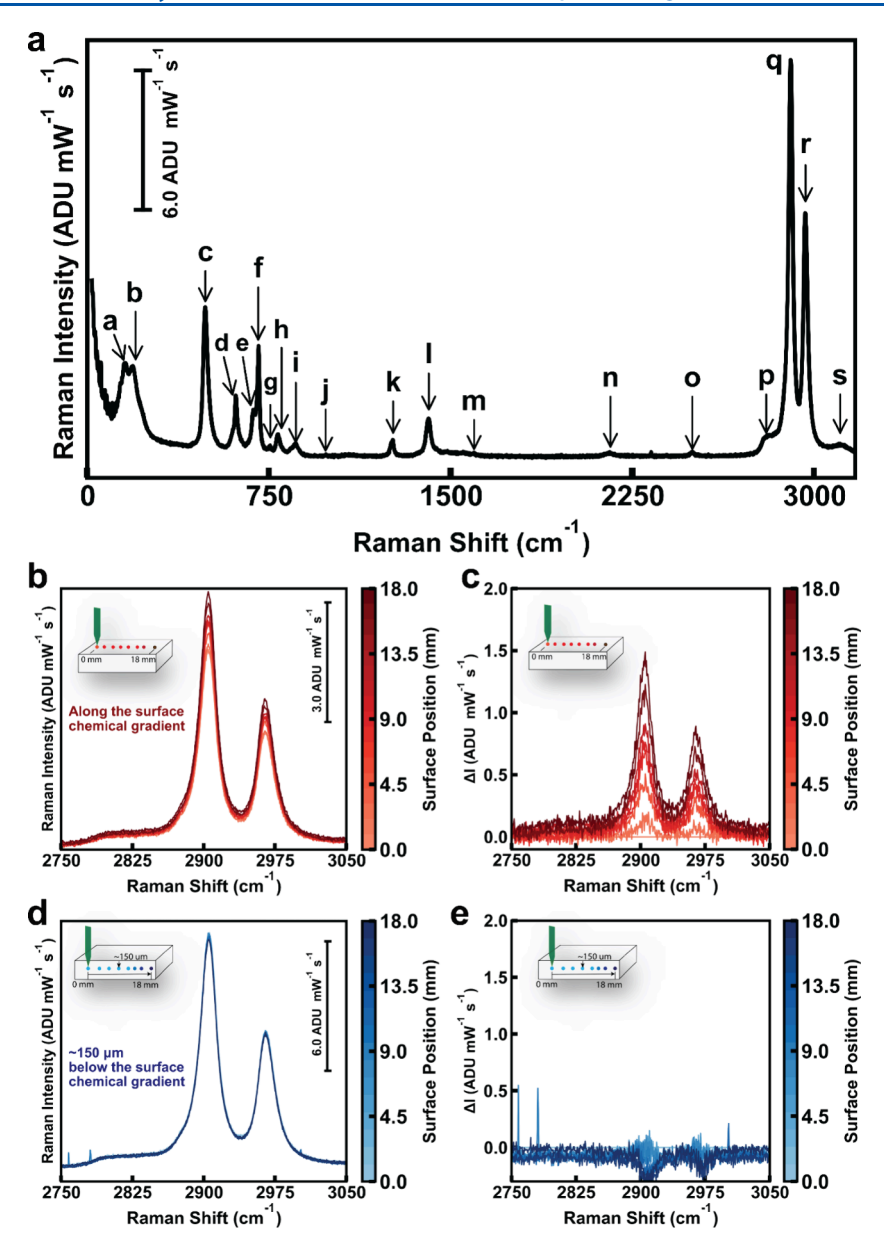


Figure 2. Observation of Raman modes on the chemically modified PDMS surface. (a) Raman spectrum of PDMS. Each mode is labeled with a letter from a to s. Details of mode assignment are available in Table S1. From (b) to (e), the CH₃ symmetric and asymmetric stretch modes q and r are chosen as spectral representative features. (b) Surface Raman spectra along the surface chemical gradient. Surface position value is arbitrarily defined to increase in the same direction as surface hydrophobicity increases. (c) Surface Raman spectral difference between consecutive positions along the surface chemical gradient. As hydrophobicity decreases, Raman intensity increases. (d) Bulk Raman spectra measured from ~150 μ m below the PDMS surface, along the chemical gradient. (e) Bulk Raman spectral difference between consecutive positions, measured ~150 μ m underneath the surface chemical gradient, showing constant spectral intensities at all positions.

of surface chemical gradients, as shown by previous studies. 32,33

We use decyltrichlorosilane (DTS) with a ten-carbon-long alkane chain to chemically modify the oxygen-plasma-activated PDMS surface. The extent of this reaction at the gas—solid interface depends on the DTS partial pressure in the gas phase. We designed a reaction chamber (Figure 1a) to produce and sustain a steady-state gradient distribution of DTS partial pressure, which translates into the DTS surface chemical gradient (Figure 1b). The end that has a higher amount of DTS deposited can be expected to be more hydrophobic, and the end with less DTS deposited is expected to be more hydrophilic. Figure 1c illustrates the contact angle variation

along the direction of the chemical gradient of the surface silane concentration.

The chemical states of interfacial molecular components are expected to vary according to the chemical gradient. We hypothesize that such surface chemical state variations will be encoded into local spectroscopic responses. This work explores the use of Raman spectroscopy as a spectroscopic tool to reveal surface chemical information.³⁴ Figure 2a shows the Raman spectrum of PDMS observed under ambient conditions excited using a 532 nm laser. We assign letter symbols from *a* to *s* to denote the observed Raman modes and follow previous literature to ascribe these modes to specific molecular motions (Supporting Information Table S1). Specifically, the *q* and *r* modes arise from the CH₃ symmetric and asymmetric

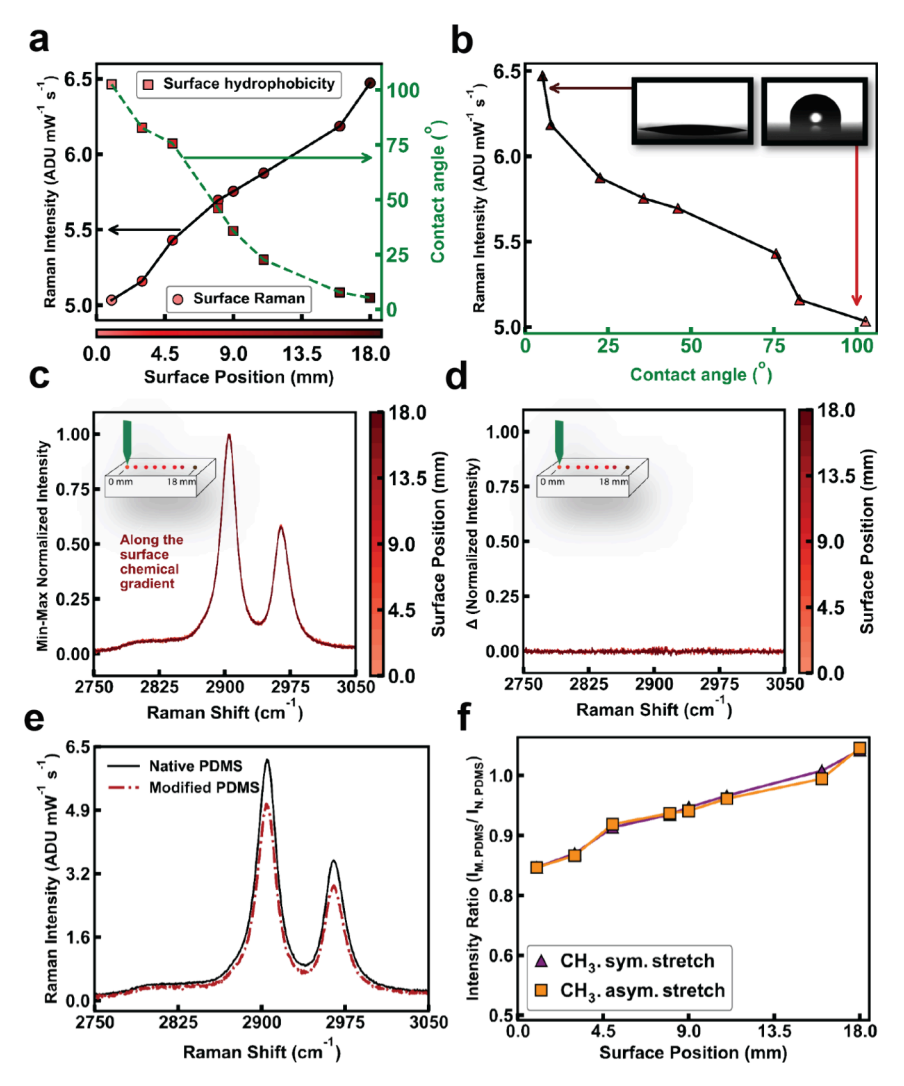


Figure 3. Raman signatures of surface chemical gradient. (a) and (b) Anticorrelation between surface Raman intensity and hydrophobicity. Surface Raman intensity decreases as the surface becomes more hydrophobic. (c) Overlay of min-max normalized surface Raman spectra across the chemical gradient. All spectra overlap exactly and do not vary in peak position and width. (d) Spectral difference of min-max normalized surface Raman spectra, showing complete overlap. (e) Raman spectra of chemically modified and native PDMS surfaces. Surface Raman intensity is suppressed after chemical modification. (f) Raman intensity ratio between chemically modified and native PDMS surfaces. The most hydrophobic region shows surface Raman intensity suppressed to about 80% of the native surface.

stretching and are the strongest modes observed. $^{35-37}$ We first analyze and discuss the q and r modes before generalizing our findings to the full spectral range. We expect that systematic variations of line width, spectral shift, and peak intensity of Raman modes will occur and correlate with surface chemical modifications.

We indeed observed systematic variations in the Raman spectra collected along the surface chemical gradient, as shown in Figures 2b and 2c. The surface chemical gradient, implemented as previously described, renders the elastomer surface increasingly hydrophobic along the direction of increasing exposure to surface capping reagent. When scanning the laser focal spot from the hydrophobic to the hydrophilic end on the elastomer surface, an excess of Raman scattering intensity was observed. For clarity, we use the symmetric and antisymmetric stretching modes q and r of the terminal methyl group as spectral representatives to discuss this systematic spectral variation. S5,38,39 Figures 2b and 2c show the background-subtracted Raman spectra and the differential spectra, respectively. The remaining spectral regions show the

same behavior, with slightly different signal strength variations (discussed later in our analysis). As a control experiment, we probed the Raman response of bulk PDMS, shown in Figures 2d and 2e. Sampled locations of bulk PDMS were chosen to be $\sim\!150~\mu\mathrm{m}$ beneath the surface right under the measured spots shown in Figures 2b and 2c. When scanning inside the bulk, we observed no spectral variation along the direction of the surface chemical gradient; the Raman spectra from all locations are virtually identical. This set of control spectra benchmarks the reproducibility of measured spectral intensities under our experimental conditions and serves as a consistency check to substantiate the robustness of our observations of surface Raman spectral variations.

Intuitively, one might expect spectral variations to originate from surface chemical modifications. Surface capping molecules possess new molecular structures and increase the local density of hydrocarbons as well as organosilicon. As they are differentially introduced to the surface locations, one would reasonably expect the hydrophobic regions to exhibit (1) stronger Raman intensities from the increased local density of

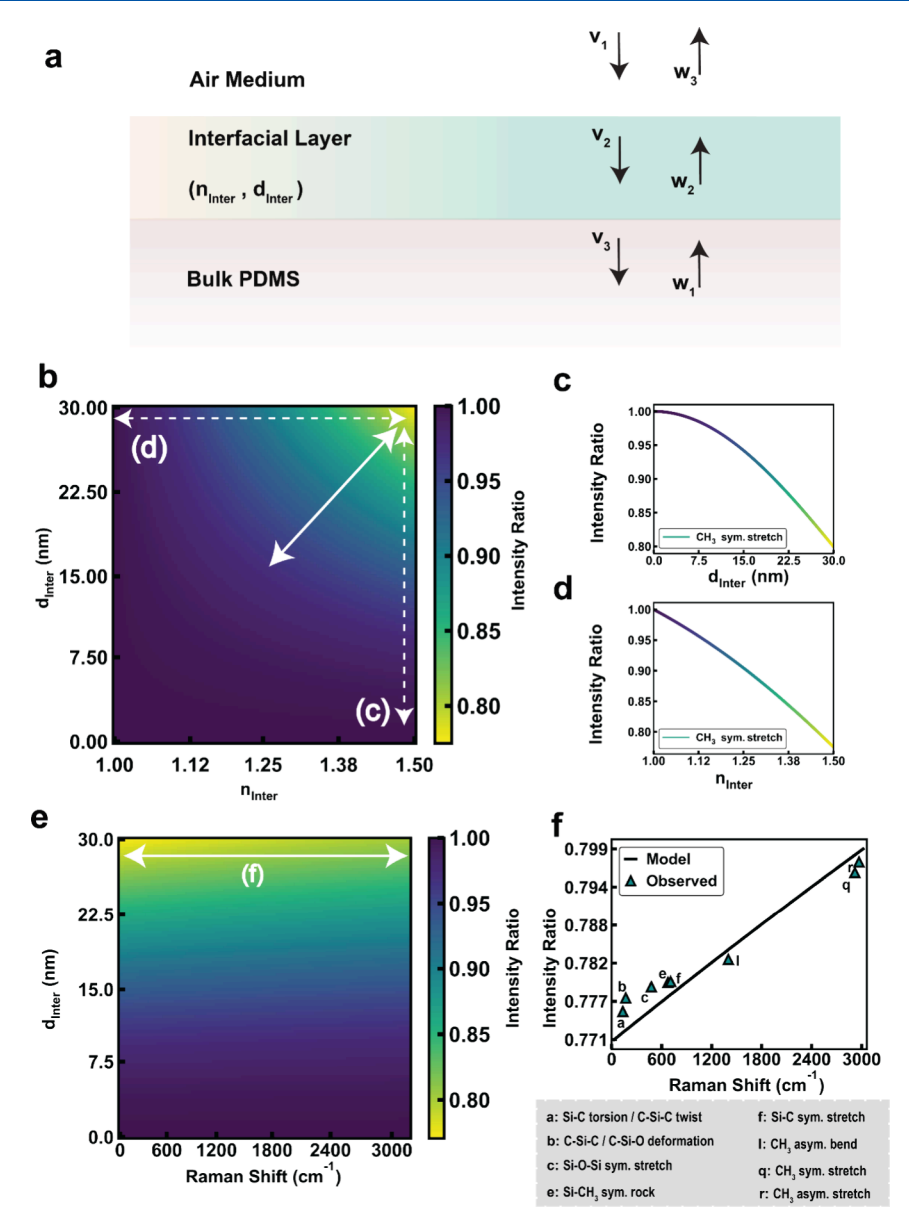


Figure 4. Optical interference modeling of the chemically modified elastomer surface. (a) Interfacial structure used in the interference model. n_{inter} and d_{inter} denote interfacial layer refractive index and thickness, respectively. Normal incidence is assumed. v_n and w_n (n=1,2,3) represent the amplitude of the forward and backward propagating wave in layer n. (b) 2D mapping of predicted Raman intensity ratio at given interfacial layer refractive index n_{inter} and thickness d_{inter} . Vertical and horizontal dashed lines, labeled with (c) and (d), correspond to the intensity ratio sectional profiles plotted in (c) and (d), respectively. The diagonal solid line represents a plausible scenario for the actual chemically modified interface, where both n_{inter} and d_{inter} increase as DTS density increases, producing an intensity suppression to \sim 80%. (c) 1D line profile of predicted Raman intensity ratio as a function of interfacial layer thickness value corresponds to the most hydrophobic region. (d) 1D line profile of predicted Raman intensity ratio as a function of interfacial layer refractive index, at a constant thickness. The largest refractive index value corresponds to the most hydrophobic region. (e) 2D mapping of predicted Raman intensity ratio at given Raman shift and interfacial layer thickness. The solid line corresponds to the line profile shown in (f). (f) Predicted and observed Raman intensity ratio as a function of Raman shift. Solid line shows predicted Raman intensity ratio at a constant interfacial layer thickness of 30 nm (soild line). Triangles show measured Raman intensity ratio of various vibrational modes.

Raman scatterers and/or (2) additional Raman features due to the presence of new chemical entities. Contrary to the chemical intuitions, however, our observations contradict both naïve expectations and show the opposite correlation between Raman intensity and surface hydrophobicity.

First, we observe an *anti*-correlation between the surface hydrophobicity and Raman intensity. The more hydrophobic surface region exhibits weaker Raman intensity despite harboring more organic capping molecules; the more hydrophilic surface region, on the other hand, exhibits stronger

Raman intensity. Figures 3a and 3b illustrate this counterintuitive intensity-hydrophobicity correlation. This correlation alone suggests that our naïve interpretation of how surface chemical modification affects its Raman response is insufficient and incapable of accounting for experimental observations.

Second, the Raman intensity is the *only* variant among Raman spectra collected from regions of different surface chemical states. Vibrational mode frequency and line width are intrinsic spectral features that sensitively reflect local physical and chemical properties of the underlying material and

molecular systems. They are robust against extrinsic factors and are extensively used as spectral markers. In our observations, all Raman spectra share identical spectral line shapes including peak position and line width. Figure 3c shows an overlay of the min-max normalized surface Raman spectra along the chemical gradient. Figure 3d shows that all differential spectra are virtually flat zero, indicating an invariant spectral line shape under different surface hydrophobicity. The absence of any change in the spectral line shape suggests that our measurements are insensitive to the specific nature of underlying chemical entities. Indeed, even when a confocal optical scheme is used to restrict the probe volume, signals from surface molecules are easily overwhelmed by those from the bulk.

Third, the surface Raman intensity overall is *suppressed* after chemical modification rather than increased by the organic molecules added to the surface. As a further control experiment, we compare the surface Raman response between native PDMS and chemically modified PDMS. The native PDMS surface has not undergone either oxygen plasma activation or DTS capping. Figures 3e and f show the spectral comparison and Raman intensity ratio as a function of surface hydrophobicity. In the most hydrophilic region, the Raman intensity is on par with that of the native surface. As the PDMS surface becomes more hydrophobic from increasing surface capping by organic molecules, its Raman response decreases to about 80% in the most hydrophobic position.

All three behaviors discussed above suggest that the origin of the observed surface Raman intensity variations, while correlated with surface chemical gradients, might not come directly from the added chemicals. Rather, a physical mechanism that is insensitive to the specific nature of the underlying chemicals is at work to produce spectral intensity variations from the materials' interface. Optical interference is one such physical mechanism.^{16,40} We next investigated the effect of optical interference on the spectral signal intensity from the interface.

Optical interference originates from the coherent interaction between light waves. When two or more phase-coherent light waves simultaneously pass through the same spatial region or reflect from the same interface, their electromagnetic fields superimpose to produce a modified total field amplitude. Constructive (destructive) interference occurs when electromagnetic fields add coherently in the phase (out of phase). The phase relationship between coherent optical field components can be sensitively controlled by nanoscale variations in optical path lengths. Consequently, the observed light intensity, quadratically dependent on the magnitude of the amplitude, exhibits strong modulation in spatial or spectral domains by interference from sometimes subtle variations of optical path characteristics. 16 In the context of materials and their interfaces, optical interference plays a crucial role in a plethora of areas. For example, optical interference served as the key mechanism generating optical contrast that enabled the discovery of single-layer graphene, 41 as well as the characterization of molecular intercalates in 2D materials. 42 Furthermore, optical interference modulates the signal strength in Raman spectroscopy in the characterization of 2D materials. 16 Recently it has also been incorporated as a signal enhancement mechanism for surface- and tip-enhanced Raman spectroscopy.⁴³

For 2D, layered, and bulk isotropic materials that are uniform along the XY directions, the system is defined by a

stack of materials with different thicknesses (d_i) and refractive indices $(n_{i,\lambda})$ along the Z direction, with i being the layer number. This produces a 1D optical system that is analytically solvable. For simple structures with few interfaces, the reflection, transmission, and multibeam interference can be accounted for using Fresnel equations. ^{16,41,44} For more complex structures with multiple interfaces, the transfer matrix method provides a more compact and general framework to model arbitrary optical characteristics of the system. ^{45–47} Next, we used the transfer matrix method to model the Raman response of a chemically modified elastomer surface.

Figure 4 shows the schematics of our optical model and the results of the calculations by using the transfer matrix method. Figure 4a depicts the structural model of our system with three layers and one nanoscale interfacial layer between two semi-infinite media of air and PDMS. Bare PDMS was used as the reference system to calculate the intensity ratio. In this model, the most important optical parameters are the refractive index and thickness of the interfacial layer. We systematically varied the values of these two parameters and predicted the Raman intensity ratio with respect to the reference case. Figure 4b shows the results of this exhaustive mapping of the two-dimensional parameter space and provides a comprehensive overview of the spectral behavior of interfacial interference.

Physically, this model predicts a general behavior that, as the interfacial layer gets thicker and/or denser, the Raman intensity decreases as compared to bare PDMS. To illustrate this behavior, Figure 4c shows the Raman intensity progression as the interfacial layer thickness d_{inter} grows from 0 to 30 nm with an assumed refractive index of 1.4572 (corresponding to the vertical line section "(c)" indicated in Figure 4b). Figure 4d shows the Raman intensity progression as the interfacial layer's refractive index n_{inter} changes from 1.00 to 1.50 with an assumed thickness of 30 nm (corresponding to the horizontal line section "(d)" indicated in Figure 4b). In both cases, the Raman intensity is suppressed to about 0.80 of the reference level, in quantitative agreement with our experimental observations. We note that both line sections of thickness d_{inter} and refractive index n_{inter} cover ranges that are too wide to be physically realistic for the PDMS interfacial layer. A physically reasonable scenario is qualitatively represented by the solid line in Figure 4b, in which both parameters of the interfacial layer evolve together, along an overall diagonal trajectory in the 2D parameter space from the lower left region (smaller d_{inter} and n_{inter}) toward the upper right region (larger d_{inter} and n_{inter}). Put another way, both interfacial thickness and refractive index evolve together during surface modifications, and they compensate for each other by altering the optical path length such that a 20% intensity variation is produced with each parameter spanning a small range.

Chemically, our optical interference model provides guidance for the structural interpretation of interfacial reactions in PDMS surface modifications. Revisiting Figure 1, the surface activation by oxygen plasma treatment creates a porous glassy layer on the PDMS surface.²⁹ This porous glassy layer is a random network of silica units with molecular scale voids resulting from the removal of methyl groups in PDMS. When exposed to capping molecules to generate the surface chemical gradient, the organic long-chain silane molecules impregnate the glassy layer and bond into the silica network via condensation reactions. This reaction produces the following effects. First, the molecular scale voids become filled with silane with long-chain hydrocarbons. This increases the local

effective refractive index. Second, the incorporation of organic silanes reduces the average connectivity of the silica network. Commonly, silicon atoms are bonded tetrahedrally with four Si–O bonds in the silica network. Silicon atoms introduced from the capping group each contribute three Si–O bonds to the network. After the reaction, the local silica network hosts more silica units with reduced bond connectivity on average, leading to a volume expansion at the nanoscale and an increase in the thickness of the interfacial layer.

The validity of our optical model is further tested in predicting the wavelength (or equivalently the Raman shift) dependence of the Raman intensity ratio, as shown in Figure 4e,f. Our previous discussions focused on the C-H symmetric and asymmetric stretching of methyl groups as strong representative modes. We now extend our investigation to broader spectral regions. Moving toward lower frequencies, we consider CH3 asymmetric bending, Si-C symmetric stretching, Si-CH₃ symmetric rocking, Si-O-Si symmetric stretching, C-Si-C/C-Si-O deformation, and Si-C torsion/C-Si-C twisting modes (Additional information on corresponding modes can be found in the Supporting Information Figure S2 and Table S1). Incorporating wavelength-dependent refractive indices, we map the 2D parameter space of the interfacial layer thickness and Raman shift, as shown in Figure 4e. We compare experimentally observed intensity ratios across the modes with respect to our model predictions and find good agreement, as shown in Figure 4f (Supporting Information Figure S8). The above structural and spectral investigations show that our optical modeling of interference quantitatively captures the observed effects of surface chemical modification on its Raman response.

Finally, we note that the optical interference mechanism of spectroscopic contrast is, in principle, universally applicable to different materials and molecules. This opens the possibility of probing the surface chemical states of elastomer devices under fluid mediums in situ or even operando. In practice, the caveat is that the identification of surface chemical states via spectral intensity relies on the dielectric contrast between the mediums. As an example, we investigate the PDMS interface underwater (Supporting Information Figure S7). Replacing air with water reduces the contrast of refractive indices against PDMS and its interface. Consequently, we predict a finite, albeit small, intensity modulation of a few percent. While this narrow margin will be challenging to quantitively measure in practice, we envision that additional layer(s) in the stack structure will enhance the interference effect and enable in situ or operando measurements.

In summary, we observed systematic spectral variations from modified elastomer surfaces with a chemical gradient. The more heavily chemically modified regions become more hydrophobic and exhibit further suppressed Raman intensity. Interestingly, only the scattering intensity varies with the chemical gradient; the frequencies and line widths of all modes remain invariant. A simple proportional accounting of the Raman scattering intensity to the underlying molecular content fails to explain the experimental findings. Optical interference produced by the chemically created interfacial layer at the nanoscale quantitatively reproduces the observed spectral behaviors. Analysis of the interfacial layer optical parameters points to molecular filling and swelling of the interfacial glassy layer of the chemically treated elastomer surface. Sensitive characterization of local chemical states of the elastomer surface has been challenging, given the interfacial complexity as well as light molecular components and labile bonding. Our work provides a facile noncontact optical method to probe the local chemical states of the elastomer interface at the micro and nanoscale. These findings reflect an informationally rich interplay between interfacial nanostructure and the distribution of chemical species within it, hinting at future implementations of this technique that can access greater levels of functional group specificity (e.g., those reflected by differences in dielectric permittivity) as well as the opportunity for optimized multidimensional space mapping.

ASSOCIATED CONTENT

Supporting Information

The Supporting Information is available free of charge at https://pubs.acs.org/doi/10.1021/acs.jpclett.4c01620.

Table S1, observations of Raman modes of polydimethylsiloxane (PDMS) at ambient conditions. Figures S1 to S8 contain additional Raman spectra of chemically modified PDMS surface and bulk, Raman observation on chemically modified PDMS surface considering all Raman modes between 18 to 3200 cm-1, surface modification using different concentrations of Silane sources (for 1:2 and1:8 ratios) with its Raman spectra and contact angle information, consistency checks of the Raman interference model, additional information on the optical interference calculations using transfer matrix method, and correlation between predicted and experimental Raman intensity ratio at interfacial layer with 30 nm thickness (PDF)

AUTHOR INFORMATION

Corresponding Authors

Stephen A. Morin — Department of Chemistry, University of Nebraska-Lincoln, Lincoln, Nebraska 68588, United States; orcid.org/0000-0002-8652-0511; Email: smorin2@unl.edu

Yinsheng Guo − Department of Chemistry, University of Nebraska-Lincoln, Lincoln, Nebraska 68588, United States; orcid.org/0000-0002-0571-8447; Email: yinshengguo@unl.edu

Authors

Dhanusha T.N. Rathnayake — Department of Chemistry, University of Nebraska-Lincoln, Lincoln, Nebraska 68588, United States

Nabeeha Malik – Department of Chemistry, University of Nebraska-Lincoln, Lincoln, Nebraska 68588, United States Sam Milone – Department of Chemistry, University of Nebraska-Lincoln, Lincoln, Nebraska 68588, United States

Complete contact information is available at: https://pubs.acs.org/10.1021/acs.jpclett.4c01620

Author Contributions

Yinsheng Guo and Stephen A. Morin conceived the research. Dhanusha T.N. Rathnayake carried out imaging and Raman spectroscopy measurements and analyzed the data. Nabeeha Malik and Sam Milone carried out sample preparation and water contact angle measurements. Dhanusha T.N. Rathnayake carried out optical modeling at the interfaces using the transfer matrix method. Yinsheng Guo, Dhanusha T.N. Rathnayake, Nabeeha Malik, and Stephen A. Morin wrote the manuscript.

All the authors discussed the data and contributed to the manuscript.

Notes

The authors declare no competing financial interest.

ACKNOWLEDGMENTS

This work is supported by the National Science Foundation/EPSCoR RII Track-1: Emergent Quantum Materials and Technologies (EQUATE), Award OIA-2044049. The research was performed in part in the Nebraska Nanoscale Facility: National Nanotechnology Coordinated Infrastructure and the Nebraska Center for Materials and Nanoscience (NCMN) and Nano-Engineering Research Core Facility (NERCF), which are supported by the National Science Foundation under Award ECCS: 2025298, and the Nebraska Research Initiative.

REFERENCES

- (1) Sidorenko, A.; Krupenkin, T.; Taylor, A.; Fratzl, P.; Aizenberg, J. Reversible Switching of Hydrogel-Actuated Nanostructures into Complex Micropatterns. *Science* (1979) **2007**, 315 (5811), 487–490.
- (2) Kapitan, J. M.; Minnick, G.; Watts, B. P.; Huang, N.; Rose, M. A.; Yang, R.; Morin, S. A. Photografting of Surface-Assembled Hydrogel Prepolymers to Elastomeric Substrates for Production of Stimuli-Responsive Microlens Arrays. *Adv. Funct Mater.* **2024**, *34* (3), No. 2305711, DOI: 10.1002/adfm.202305711.
- (3) Bowen, J. J.; Rose, M. A.; Morin, S. A. Surface Molding of Multi-Stimuli-Responsive Microgel Actuators. *MRS Bull.* **2021**, *46* (4), 337–344.
- (4) Mazaltarim, A. J.; Torres, A.; Morin, S. A. Mechanically Tunable Superhydrophobic Surfaces Enabled by the Rational Manipulation of Microcrack Networks in Nanoporous Films. *Adv. Mater. Interfaces* **2021**, *8* (17), No. 2100869, DOI: 10.1002/admi.202100869.
- (5) Clegg, J. R.; Peppas, N. A. Molecular Recognition with Soft Biomaterials. *Soft Matter* **2020**, *16* (4), 856–869.
- (6) Cianchetti, M.; Laschi, C.; Menciassi, A.; Dario, P. Biomedical Applications of Soft Robotics. *Nat. Rev. Mater.* **2018**, *3* (6), 143–153.
- (7) Stuart, M. A. C.; Huck, W. T. S.; Genzer, J.; Müller, M.; Ober, C.; Stamm, M.; Sukhorukov, G. B.; Szleifer, I.; Tsukruk, V. V.; Urban, M.; Winnik, F.; Zauscher, S.; Luzinov, I.; Minko, S. Emerging Applications of Stimuli-Responsive Polymer Materials. *Nat. Mater.* **2010**, *9* (2), 101–113.
- (8) Son, D.; Bao, Z. Nanomaterials in Skin-Inspired Electronics: Toward Soft and Robust Skin-like Electronic Nanosystems. ACS Nano 2018, 12 (12), 11731–11739.
- (9) Genzer, J.; Bhat, R. R. Surface-Bound Soft Matter Gradients. Langmuir 2008, 24 (6), 2294–2317.
- (10) Chaudhury, M. K.; Whitesides, G. M. How to Make Water Run Uphill. *Science* (1979) **1992**, 256 (5063), 1539–1541.
- (11) Wu, T.; Efimenko, K.; Genzer, J. Combinatorial Study of the Mushroom-to-Brush Crossover in Surface Anchored Polyacrylamide. *J. Am. Chem. Soc.* **2002**, *124* (32), 9394–9395.
- (12) Mazaltarim, A. J.; Taylor, J. M.; Konda, A.; Stoller, M. A.; Morin, S. A. Mechanically Induced Hydrophobic Recovery of Poly(Dimethylsiloxane) (PDMS) for the Generation of Surfaces with Patterned Wettability. ACS Appl. Mater. Interfaces 2019, 11 (36), 33452–33457.
- (13) Mazaltarim, A. J.; Morin, S. A. Programmable Droplet Transport Using Mechanically Adaptive Chemical Gradients with Anisotropic Microtopography. *Advanced Intelligent Systems* **2022**, *4* (4), No. 2100207, DOI: 10.1002/aisy.202100207.
- (14) Perez-Toralla, K.; Konda, A.; Bowen, J. J.; Jennings, E. E.; Argyropoulos, C.; Morin, S. A. Rational Synthesis of Large-Area Periodic Chemical Gradients for the Manipulation of Liquid Droplets and Gas Bubbles. *Adv. Funct. Mater.* **2018**, 28 (8), No. 1705564, DOI: 10.1002/adfm.201705564.
- (15) Sun, S.; Rathnayake, D. T. N.; Guo, Y. Asymmetrical Spectral Continuum between Anti-Stokes and Stokes Scattering Revealed in

- Low-Frequency Surface-Enhanced Raman Spectroscopy. J. Phys. Chem. C 2022, 126 (27), 11193-11200.
- (16) Yoon, D.; Moon, H.; Son, Y. W.; Choi, J. S.; Park, B. H.; Cha, Y. H.; Kim, Y. D.; Cheong, H. Interference Effect on Raman Spectrum of Graphene on SiO2/Si. *Phys. Rev. B Condens Matter Mater. Phys.* **2009**, *80* (12), No. 125422, DOI: 10.1103/PhysRevB.80.125422.
- (17) Wolf, M. P.; Salieb-Beugelaar, G. B.; Hunziker, P. PDMS with Designer Functionalities—Properties, Modifications Strategies, and Applications. *Prog. Polym. Sci.* **2018**, *83*, 97–134.
- (18) Prajzler, V.; Nekvindova, P.; Spirkova, J.; Novotny, M. The Evaluation of the Refractive Indices of Bulk and Thick Polydimethylsiloxane and Polydimethyl-Diphenylsiloxane Elastomers by the Prism Coupling Technique. *Journal of Materials Science: Materials in Electronics* **2017**, 28 (11), 7951–7961.
- (19) Schneider, F.; Draheim, J.; Kamberger, R.; Wallrabe, U. Process and Material Properties of Polydimethylsiloxane (PDMS) for Optical MEMS. Sens Actuators A Phys. 2009, 151 (2), 95–99.
- (20) Polyanskiy, M. N. Refractiveindex.Info Database of Optical Constants. Sci. Data 2024, 11 (1). DOI: 10.1038/s41597-023-02898-2
- (21) Tan, A.; Pellegrino, L.; Cabral, J. T. Tunable Phase Gratings by Wrinkling of Plasma-Oxidized PDMS: Gradient Skins and Multiaxial Patterns. ACS Appl. Polym. Mater. 2021, 3 (10), 5162–5170.
- (22) Arosa, Y.; de la Fuente, R. Refractive Index Spectroscopy and Material Dispersion in Fused Silica Glass. *Opt. Lett.* **2020**, 45 (15), 4268–4271.
- (23) Wang, Z.; Luo, Y.; Zheng, F.; Zhang, N.; Yin, C.; Li, J.; He, C.; Peng, X.; Huang, Z.; Fang, P. Study on Surface Structure of Plasma-Treated Polydimethylsiloxane (PDMS) Elastomer by Slow Positron Beam. Surf. Interface Anal. 2018, 50 (8), 819–826.
- (24) Miranda, I.; Souza, A.; Sousa, P.; Ribeiro, J.; Castanheira, E. M. S.; Lima, R.; Minas, G. Properties and Applications of PDMS for Biomedical Engineering: A Review. *J. Funct Biomater* **2022**, *13* (1), 2.
- (25) Van Poll, M. L.; Zhou, F.; Ramstedt, M.; Hu, L.; Huck, W. T. S. A Self-Assembly Approach to Chemical Micropatterning of Poly-(Dimethylsiloxane). *Angewandte Chemie International Edition* **2007**, 46 (35), 6634–6637.
- (26) Berthier, E.; Young, E. W. K.; Beebe, D. Engineers Are from PDMS-Land, Biologists Are from Polystyrenia. *Lab Chip* **2012**, *12* (7), 1224–1237.
- (27) Trantidou, T.; Elani, Y.; Parsons, E.; Ces, O. Hydrophilic Surface Modification of Pdms for Droplet Microfluidics Using a Simple, Quick, and Robust Method via Pva Deposition. *Microsyst. Nanoeng.* **2017**, 3 (1), No. 16091, DOI: 10.1038/micronano.2016.91.
- (28) Wagner, J. R.; Fletcher, J.; Morin, S. A. Chemical Activation of Commodity Plastics for Patterned Electroless Deposition of Robust Metallic Films. *Chem. Commun.* **2022**, *58* (74), 10337–10340.
- (29) Béfahy, S.; Lipnik, P.; Pardoen, T.; Nascimento, C.; Patris, B.; Bertrand, P.; Yunus, S. Thickness and Elastic Modulus of Plasma Treated PDMS Silica-like Surface Layer. *Langmuir* **2010**, *26* (5), 3372–3375.
- (30) Gokaltun, A.Ih.; Kang, Y. B.; Yarmush, M. L.; Usta, O. B.; Asatekin, A. Simple Surface Modification of Poly(Dimethylsiloxane) via Surface Segregating Smart Polymers for Biomicrofluidics. *Sci. Rep.* **2019**, 9 (1). DOI: 10.1038/s41598-019-43625-5.
- (31) Rao, L.; Liu, Y.; Zhou, H. Significantly Improved Cell Affinity of Polydimethylsiloxane Enabled by a Surface-Modified Strategy with Chemical Coupling. *J. Mater. Sci. Mater. Med.* **2022**, 33 (10). DOI: 10.1007/s10856-022-06690-3.
- (32) Efimenko, K.; Genzer, J. How to Prepare Tunable Planar Molecular Chemical Gradients. *Adv. Mater.* **2001**, *13* (20), 1560–1563.
- (33) Mohan, G.; Gallant, N. D. Surface Chemistry Gradients on Silicone Elastomers for High-Throughput Modulation of Cell-Adhesive Interfaces. *J. Biomed Mater. Res. A* **2015**, *103* (6), 2066–2076.
- (34) Xu, Z.; He, Z.; Song, Y.; Fu, X.; Rommel, M.; Luo, X.; Hartmaier, A.; Zhang, J.; Fang, F. Topic Review: Application of

- Raman Spectroscopy Characterization in Micro/Nano-Machining. *Micromachines (Basel)* **2018**, 9 (7), 361.
- (35) Jayes, L.; Hard, A. P.; Séné, C.; Parker, S. F.; Jayasooriya, U. A. Vibrational Spectroscopic Analysis of Silicones: A Fourier Transform-Raman and Inelastic Neutron Scattering Investigation. *Anal. Chem.* **2003**, 75 (4), 742–746.
- (36) Alshehri, A. M.; Deepak, K. L. N.; Marquez, D. T.; Desgreniers, S.; Bhardwaj, V. R. Localized Nanoclusters Formation in PDMS upon Irradiation with Femtosecond Laser. *Opt Mater. Express* **2015**, 5 (4), 858–869.
- (37) Bae, S. C.; Lee, H.; Lin, Z.; Granick, S. Chemical Imaging in a Surface Forces Apparatus: Confocal Raman Spectroscopy of Confined Poly(Dimethylsiloxane). *Langmuir* **2005**, *21* (13), 5685–5688.
- (38) Bokobza, L. Some Applications of Vibrational Spectroscopy for the Analysis of Polymers and Polymer Composites. *Polymers (Basel)* **2019**, *11* (7), 1159.
- (39) Bokobza, L.; Bruneel, J. L.; Couzi, M. Raman Spectroscopy as a Tool for the Analysis of Carbon-Based Materials (Highly Oriented Pyrolitic Graphite, Multilayer Graphene and Multiwall Carbon Nanotubes) and of Some of Their Elastomeric Composites. *Vib Spectrosc* **2014**, *74*, 57–63.
- (40) Liu, K.; Gong, T.; Luo, Y.; Kong, W.; Yue, W.; Wang, C.; Luo, X. Ultrasensitive Enhanced Raman Spectroscopy by Hybrid Surface-Enhanced and Interference-Enhanced Raman Scattering with Metal-Insulator-Metal Structures. *Opt Express* **2023**, *31* (10), 15848–15863.
- (41) Blake, P.; Hill, E. W.; Castro Neto, A. H.; Novoselov, K. S.; Jiang, D.; Yang, R.; Booth, T. J.; Geim, A. K. Making Graphene Visible. *Appl. Phys. Lett.* **2007**, *91* (6), No. 063124, DOI: 10.1063/1.2768624.
- (42) Jung, N.; Crowther, A. C.; Kim, N.; Kim, P.; Brus, L. Raman Enhancement on Graphene: Adsorbed and Intercalated Molecular Species. *ACS Nano* **2010**, *4* (11), 7005–7013.
- (43) Guo, Y.; Jiang, S.; Chen, X.; Mattei, M.; Dieringer, J. A.; Ciraldo, J. P.; Van Duyne, R. P. Using a Fabry-Perot Cavity to Augment the Enhancement Factor for Surface-Enhanced Raman Spectroscopy and Tip-Enhanced Raman Spectroscopy. *J. Phys. Chem. C* **2018**, *122* (26), 14865–14871.
- (44) Born, M.; Wolf, E. Principles of Optics; Electromagnetic Theory of Propagation. In *Interference and Diffraction of Light*, 7th ed.; Cambridge University Press: Cambridge, UK, 1997.
- (45) Katsidis, C. C.; Siapkas, D. I. General Transfer-Matrix Method for Optical Multilayer Systems with Coherent, Partially Coherent, and Incoherent Interference. *Appl. Opt.* **2002**, *41* (19), 3978–3987.
- (46) Troparevsky, M. C.; Sabau, A. S.; Lupini, A. R.; Zhang, Z. Transfer-Matrix Formalism for the Calculation of Optical Response in Multilayer Systems: From Coherent to Incoherent Interference. *Opt Express* **2010**, *18* (24), 24715–24721.
- (47) Byrnes, S. J. Multilayer Optical Calculations. *arXiv*. 2016. DOI: 10.48550/arXiv.1603.02720.